Accepted Manuscript

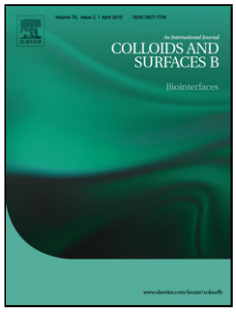

Title: Ultrafast fabrication of thermally stable protein-coated silver iodide nanoparticles for solid-state superionic conductors

Authors: Aryane Tofanello, Juscemácia N. Araujo, Iseli L. Nantes-Cardoso, Fabio F. Ferreira, José A. Souza, Dae-Woon Lim, Hiroshi Kitagawa, Wanius Garcia

PII: S0927-7765(18)30939-1
DOI: https://doi.org/10.1016/j.colsurfb.2018.12.059
Reference: COLSUB 9913

To appear in: *Colloids and Surfaces B: Biointerfaces*

Received date: 5 July 2018
Revised date: 28 September 2018
Accepted date: 20 December 2018

Please cite this article as: Tofanello A, Araujo JN, Nantes-Cardoso IL, Ferreira FF, Souza JA, Lim D-Woon, Kitagawa H, Garcia W, Ultrafast fabrication of thermally stable protein-coated silver iodide nanoparticles for solid-state superionic conductors, *Colloids and Surfaces B: Biointerfaces* (2018), https://doi.org/10.1016/j.colsurfb.2018.12.059

Ultrafast fabrication of thermally stable protein-coated silver iodide nanoparticles for solid-state superionic conductors

Aryane Tofanello[a], Juscemácia N. Araujo[a], Iseli L. Nantes-Cardoso[a], Fabio F. Ferreira[a], José A. Souza[a], Dae-Woon Lim[b], Hiroshi Kitagawa[b,c], Wanius Garcia[a,*]

[a] Centro de Ciências Naturais e Humanas, Universidade Federal do ABC (UFABC), Santo André, SP, Brazil

[b] Division of Chemistry, Graduate School of Science, Kyoto University, Kitashirakawa-Oiwakecho, Sakyo-ku, Kyoto, Japan

[c] INAMORI Frontier Research Center, Kyushu University, 744 Motooka, Nishi-ku, Fukuoka 819-3095, Japan

* E-mail: wanius.garcia@ufabc.edu.br

Short statistical summary of the article:

Total number of words: 5,690

Total number of tables: 0

Total number of figures: 8

Graphical abstract

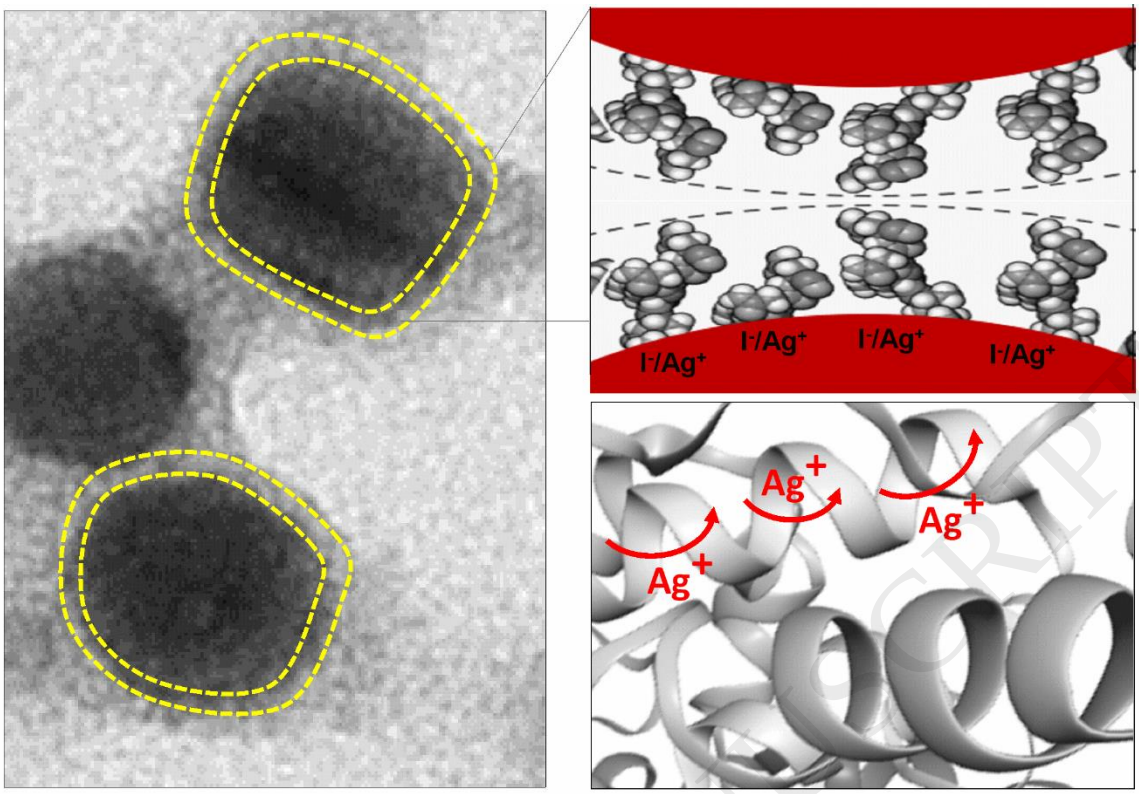

Highlights

- Ultrafast synthesis of thermally stable protein-coated AgI nanoparticles (NPs)
- Transition from the α- to β-/γ-phase was drastically suppressed
- Thermally stable organic-inorganic hybrid system with superionic conductivity
- Superionic conductivity of protein/AgI NPs is maintained during thermal cycles
- Diffusion of mobile Ag^+ on the surface of the AgI NPs through a protein matrix

Abstract

Solid-state ionic conductor is an essential and critical part of electrochemical devices such as batteries and sensors. Nano-sized silver iodide (AgI) is the most promising ionic conductor due to its superionic conductivity at room temperature. In recent years, proteins have been used as organic templates to obtain high-performance solid-state ionic conductors as well as to extend their applications in a biosensor. Here, we report the unprecedented ultrafast synthesis of thermally stable protein-coated AgI nanoparticles (NPs) through the photo-irradiation method for solid-state electrolyte. The synthesis was performed using a hyperthermostable bacterial β-glucosidase. The protein-coated AgI NPs with an approximate diameter of 13 nm showed that the controllable transition from the α- to β-/γ-phase was drastically suppressed down to 41 ^{o}C in the cooling process. After drying, the product represents a thermally stable organic-inorganic hybrid system with superionic conductivity. It is noteworthy that the superionic conductivity ($\sigma \sim 0.14$ S/cm at 170 ^{o}C) of thermally stable protein-coated AgI NPs is maintained during several thermal cycles (25–170 °C). To our knowledge, this is the first report showing the diffusion of mobile Ag^{+} ions on the surface of the AgI NPs through a protein matrix. The facile synthesis method and high performance of the protein-coated AgI NPs may provide a latent application in the mass production of nanobatteries and other technological applications.

Keywords: Solid-state ionic conductors; AgI nanoparticles; organic-inorganic hybrid system; superionic conductivity; thermostable protein-coated; protein structure

1. Introduction

Ionic conductors are essential components in electrochemical devices due to its great stability and safety properties [1]. In general, batteries employ liquid electrolytes which cause safety problems. In order to overcome these problems, solid-state electrolytes such as silver-based ionic conductors are considered to be an alternative. In particular, silver iodide (AgI) NPs are the most promising candidate due to its superionic conductivity and polarizability [1-4]. Bulk AgI is a direct-bandgap (~ 2.9 eV) semiconductor that usually exists as a mixture of the β- and γ- poorly conducting phases (conductivity ~ 10^{-7} S/cm) under ambient conditions. The β- and γ- phases of AgI possess the hexagonal wurtzite and cubic zinc-blende crystal structures, respectively, both of which support Frenkel defects, i.e., Ag^+ vacancies and Ag^+ interstitials [5-7]. However, at 147 ^oC the bulk AgI undergoes an abrupt phase transition to α-phase with superionic behavior (conductivity greater than 1 S/cm), in which iodine ions are arranged in a body-centered cubic (bcc) lattice, with highly mobile Ag^+ randomly distributed through the interstices [8].

One of the ways to stabilize the superionic AgI α-phase at lower temperatures is the fabrication of AgI nanoconductors with controlled size and shape since the reduced particle size causes a large hysteresis of phase transition temperature in the heating and cooling processes [9]. Therefore, the synthesis of AgI nanoconductors has attracted considerable interest in many fields of science and technology owing to their unusual physical and chemical properties, which are substantially different from the bulk materials [9-11]. Previously, it was reported that poly-*N*-vinyl-2-pyrrolidone(PVP)-coated AgI NPs with a diameter of ~ 11 nm presented superionic conductivity of ~ 1.5 x 10^{-2} S/cm at room temperature, five orders of magnitude higher than that of bulk AgI

[9]. Furthermore, the same study described that the transition temperature of PVP-coated AgI NPs (~ 11 nm) from the α-phase to the β-/γ-phase is 40 ^{o}C (during the cooling process), showing a significant hysteresis of approximately 100 ^{o}C, while the hysteresis for the bulk AgI is only 2.5 ^{o}C. Another study reported that the superionic conducting α-phase of PVP-coated AgI NPs was stabilized down to at least 20 ^{o}C by applying a pressure of 0.18 GPa [10]. Also, it was reported that PVP-coated AgI NPs with a diameter of ~ 3 nm did not present superionic phase transition and its ionic conductivity was lower than that of bulk AgI [11].

In recent years, green syntheses using organic materials have emerged as an alternative method to produce and stabilize nanoscale ionic conductors [12-14]. Modifications of semiconductor NPs surface with organic molecules have improved its chemical and physical properties [15-17]. Protein molecules are complex natural organic polymers, which can be used as additives to synthesize and modify new materials. However, its structural and compositional complexity is challenging to use it polymer matrix without proper manipulations. Therefore, the use of protein as the polymer matrix for ion conductors is rare. Few studies reported the use of proteins, for example gelatin and soy proteins, as the matrix for polymer ion conductors [14,18-20]. Moreover, it is well known that AgI NPs mixed with a solid insulating material will display significantly enhanced conductivity [21]. For these reasons, the use of proteins as an organic polymer matrix to obtain high-performance solid-state ionic conductors is technically challenging and has attracted considerable research interest [21].

Herein, we report, for the first time, thermally stable protein-assisted AgI NPs synthesized by photochemical route, its phase transition, and superionic conductivity. The synthesis was performed using a hyperthermostable β-glucosidase from the bacterium *Thermotoga petrophila* [13]. The product represents an organic-inorganic

hybrid system with superionic conductivity. An important goal of this study is to observe the effects of the organic contribution (protein capping) on the correlations between phase transition and ionic conductivity of the protein-coated AgI-NPs as a function of temperature.

2. Materials and methods

2.1. Synthesis of protein-coated AgI nanoparticles (protein/AgI-NPs)

The expression and purification of hyperthermostable β-glucosidase GH1 from the bacterium *Thermotoga petrophila* were carried out as described previously [22,23]. The protein-coated AgI nanoparticles (protein/AgI-NPs) were synthesized by a one-pot photochemical method. In a typical procedure, aqueous solutions of 1 mM $AgNO_3$, 1 mM KI and 2 μM of β-glucosidase GH1 were mixed and irradiated with blue light (maximum wavelength of 480 nm and total intensity of 11 mW/cm^2 at 7 cm) during 13 minutes at room temperature and without stirring. Control samples were performed under irradiation and absence of protein. A double-beam UV-VIS spectrophotometer (Biachrom Libra) was used to measure the absorbance over the wavelength range from 200 to 800 nm. The protein/AgI-NPs were washed by centrifugation with ultrapure water to remove the unbound proteins, dried overnight at 50 ^oC, and posteriorly characterized by physical methods.

2.2. Characterization of protein/AgI-NPs

The protein/AgI-NPs crystal structures were characterized using X-ray powder diffraction (XRD) technique as a function of temperature. Measurements were carried out on a STADI-P powder diffractometer (Stoe®, Darmstadt, Germany) using Cu $K\alpha_1$

radiation (λ = 1.54056 Å), with a tube voltage of 40 kV and a current of 40 mA, in the range from 20^o to 60^o (2θ), with step sizes of 0.015^o and 200 s of integration time at each 1.05^o. The size and morphology of protein/AgI-NPs were characterized using a transmission electron microscope (JEOL JEM -100CX) with an accelerating voltage of 80 kV. The samples were drop-cast onto a carbon-coated copper grid and allowed to dry at ambient conditions. Differential scanning calorimetry (DSC) measurements were carried out with a Netzsch DSC 214 Polyma instrument in the range 25–190 °C with a typical sweeping rate of 5 °C min^{-1}. The average zeta potential (ζ) value of the protein/AgI-NPs sample in ultrapure water was determined using the electrophoretic light scattering (ELS) method. The data were collected employing a Zetasizer Nano-ZS (Malvern). The A.C. conductivity measurements of the protein/AgI-NPs were carried out by the conventional two-probe method. Samples were compacted to pellets of ~ 1.0 mm thickness and 2.5 mm in diameter, and both sides covered with gold paste were connected to a Solartron SI 1260 Impedance/Gain-Phase Analyzer and 1296 dielectric interface. The impedance measurement was executed in the frequency range from 1 Hz to 1 MHz, temperature range 25–170 °C with an applied voltage of 100 mV.

3. Results and discussion

The fabrication of solid-state protein-based ionic conductor using denatured soy proteins and lithium salt ($LiClO_4$) was recently reported [14]. This hybrid conductor showed an ionic conductivity of $\sigma \sim 10^{-5}$ S/cm at room temperature, conductivity which is not applicable for practical batteries. To achieve significant improvements in conductivity, the proposed strategies are the addition of nanoparticles and more precise control of protein structures [14]. In this context, we analyzed the role of native protein

structure on the enhanced superionic properties. Thus, we report for the first time the ultrafast photosynthesis of thermally stable protein-coated silver iodide nanoparticles (protein/AgI-NPs) under blue light irradiation (Fig. 1). In the absence of protein and under irradiation no significant changes in the color of the solution were observed, confirming that AgI-NPs synthesis is not only photochemically assisted (Fig. 1B, vials 1 to 3). The reverse process also showed that the synthesis is not protein-dependent exclusively (Fig. 1B, vial 4). Only in vial 4 we observed the precipitation of silver iodide (AgI bulk) from a reaction between silver nitrate and potassium iodide. When protein (2 μM, β-glucosidase) was added in ultrapure water containing 1 mM $AgNO_3$ and 1 mM KI and irradiated with blue light, the color of the solution initially clear changed to light brown after a few minutes (Fig. 1B, vial 5), proving the formation of protein/AgI-NPs. The color of the colloidal solution remained then unaltered indicating that the protein/AgI-NPs were efficiently stabilized.

The photosynthesis of protein/AgI-NPs was monitored spectrophotometrically measuring the absorption profile as a function of time. The absorption spectra of protein/AgI-NPs showed a defined band around 420 nm, which was attributed to the characteristic band of AgI induced by the dipole forbidden transition ($4d^{10}$ to $4d^{9}5s^{1}$) allowed by the tetrahedral symmetry of the Ag^{+} ion site (Fig. 1A) [24]. The resultant p-d hybridization may be attributed to $Z_{1,2}$ excitons. At the same time, the low-resolution peak at 320 nm is due to spin-orbit split I^{-} valence of the spin-orbit interaction and may be attributed to Z_3 excitons. The band intensity at 420 nm increased up to 5 minutes and then it remained constant indicating that the photosynthesis of protein/AgI-NPs was completed in 5 minutes (right inset of Fig. 1A). In addition, the optical band gap of the protein-coated AgI nanoparticles was obtained from the maximum absorbance using the Tauc plot (Fig. S1). The estimated optical band gap energy was 2.87 eV, which is

slightly larger than that of the bulk AgI (2.78 eV) [25]. It is possible that the band gap shift occurred due to the presence of the protein capping that can have generated additional electronic states or the coexistence of β- and γ-phases.

The final yield was typically 100 mg of protein/AgI-NPs (from 1 L of colloidal solution after drying) in the form of dark powder easily moldable (Fig. S2), suggesting excellent mechanical properties. When the synthesis was carried out with a higher protein concentration (8 μM), the yield of the process was subtly larger (Fig. S3). However, when the synthesis was performed with a lower protein concentration (0.5 μM), the yield of the process decreased drastically. Thus, for equimolar mixture (1 mM $AgNO_3$ and 1 mM KI) we conclude that 2 μM was an ideal protein concentration for the optimization process of the synthesis.

After photosynthesis and purification, the morphology and dimension of protein/AgI-NPs were analyzed by transmission electron microscopy (TEM). TEM micrographs revealed that AgI-NPs formed are nearly spherical with small polydispersion in size (Fig. 2 and Fig. S4). The particle size distribution revealed that the mean diameter of AgI-NPs was 12.8 ± 4.9 nm (Fig. 2). The micrographs also showed that the AgI-NPs are embedded in a protein matrix and the observed agglutination is due to the drying process required for the samples preparation. Also, the value determined for the zeta-potential was of $\zeta = -41.2 \pm 6.5$ mV (Fig. S5) for protein/AgI-NPs confirming the role of protein as capping and stabilizing agent due to the electrostatic repulsion among adsorbed proteins [13]. Furthermore, the average size of the distance between the AgI NPs, which represents the thickness of the protein matrix, was also analyzed (Fig. 3). The mean distance between the AgI NPs was 7.5 ± 1.5 nm. The β-glucosidase GH1 forms a homodimer with 10 nm long and 5 nm wide (inset of Fig. 3) [22]. If the protein (homodimer) is “lying” on the surface of the AgI

nanoparticle, then the coating of the protein would have a thickness of approximately 5 nm. Thus, when two protein/AgI-NPs are in contact occurs the formation of a protein bilayer with a thickness of approximately 10 nm (Fig. 3). This value is in accordance with the mean distance between the AgI NPs (7.5 ± 1.5 nm), and the small discrepancy observed is due to the fact that TEM analyzes were made in dry state. Therefore, our results suggest that the AgI NPs are covered by a protein monolayer.

The phase transition and thermal response of protein/AgI-NPs were analyzed using differential scanning calorimetry (DSC) (Fig. 4). In the first thermal cycle, during the heating process, a broad endothermic peak was observed in the range between 90 and 110 ^{o}C, which may be related mainly to the water elimination [26], followed by another endothermic peak at 156 ± 1 ^{o}C related to the transition from the β-/γ- to α-phase. During the cooling process, only a single exothermic peak at 40 ± 1 ^{o}C was observed related to the transition from the α- to β-/γ-phase. Over the next three thermal cycles, a single endothermic peak at 142 ± 1 ^{o}C appeared during the heating processes, while a single exothermic peak at 41 ± 1 ^{o}C was observed during the cooling processes (Fig. 4). These results confirm that the stabilization of the α-phase at lower temperature is reversible and the process is reproducible even after four thermal cycles. From the second thermal cycle, the transition temperature from the β-/γ- to α-phase for the photosynthesized protein/AgI-NPs occurs at a lower temperature (142 ^{o}C) than that of bulk material (147 ^{o}C). Differently, for PVP-coated AgI-NPs the transition temperature from the β-/γ- to α-phase occurred at a higher temperature than observed for the bulk material [9]. The protein/AgI-NPs (mean diameter of 12.8 ± 4.9 nm) have the transition from the α- to β-/γ-phase drastically suppressed down to 41 ± 1 ^{o}C, resulting in a substantial hysteresis which in turn reveals the coexistence of crystal phases (Fig. 4). This behavior is similar to the results reported by Makiura and coworkers for PVP-

coated AgI-NPs with an average diameter of 11.3 ± 3.8 nm [9]. As previously proposed for PVP-coated AgI-NPs, the suppression of the transition from the α- to β-/γ-phase during the cooling process can be attributed to the increase of the surface energy, the presence of lattice defects, and grain boundaries in the surface region. In the α-phase, the surface region is strongly affected by defects caused by the diffusion of Ag^+ ions in the interface between the protein-coating layer and the AgI-NPs, whereas iodine ions remain on the surface of the AgI-NPs [9]. Furthermore, while the DSC peak for PVP-coated AgI-NPs (11.3 ± 3.8 nm) on the cooling process was very sharp, for protein/AgI-NPs (12.8 ± 4.9 nm) the peak was broad (Fig. 4) due to a greater polydispersity in particle size. Moreover, when the protein/AgI-NPs were sintered at 450 ^oC for 4 hours, the results of DSC were closer to those expected for the bulk AgI (Fig. 4, at the bottom). The bacterial β-glucosidase GH1 used in our syntheses is a hyperthermostable homodimeric protein (Fig. 3), which maintains structural stability even when incubated at 99 ^oC during 10 hours [22,23]. As the DSC measurements were reproducible in cycles with a maximum temperature of 190 ^oC, the results suggest that the structural stability of the protein is increased in complex with the AgI NPs. Even after incubation at 170 ^oC the protein/AgI-NPs showed residual β-glucosidase activity (data not shown). However, incubation at very high temperatures, such as 450 ^oC, should have removed the protein layer destabilizing the AgI NPs and affecting their ionic conduction properties (Fig. 4).

X-ray powder diffraction (XRD) analysis was employed to study the crystal structure and phase transition of the protein/AgI-NPs as a function of temperature. Fig. 5 shows the X-ray diffraction patterns of protein/AgI-NPs during the thermal cycling (heating and cooling processes). In agreement with the DSC analyzes, the XRD results also showed clearly the same substantial hysteresis for the transition from the α- to β-/γ-

phase. It should be mentioned that the first measurement was performed *ex-situ* at room temperature (25 ºC), which implied in a slightly different background since the powder sample was loaded between two acetate-cellulose foils. The *in-situ* experiments were performed with the sample loaded in 0.5 mm diameter glass capillaries. At room temperature, the protein/AgI-NPs is composed of a mixture of hexagonal β-AgI (35 ± 3 wt%; JCPDS card No. 09-0374) and cubic γ-AgI (65 ± 3 wt%; JCPDS card No. 09-399) phases, as shown in Fig. 6. At 40 ºC, the β-AgI (15 ± 2 wt%) phase gradually decreases with subsequent increase of the γ-AgI (85 ± 2 wt%) phase. At 170 ºC, a complete phase transformation from the mixing β-/γ-AgI phases to the single α-AgI (JCPDS card No. 20-1058) phase occurred. This behavior remained after cycling the sample to a higher temperature (190 ºC) and then to 150 ºC and 120 ºC, thus showing that transition from the β-/γ- to α-phase is strongly thermally hysteretic. During the last measurement, at 40 ºC, one can see the reappearance of the β-/γ-AgI phases with a small fraction of the α-phase is still observed, and below this temperature (which coincides with the maximum value of the endothermic peak observed in DSC analysis) the protein/AgI-NPs undergoes a rapid transition to the β-/γ- phase.

The superionic conductivity of protein/AgI-NPs was verified by the alternating current (A.C.) impedance measurement. Fig. 7 shows the results of conductivity measurements for protein/AgI-NPs with a diameter of 12.8 ± 4.9 nm. Again, the significant thermal hysteretic behavior observed in DSC and DRX analyzes was observed in conductivity measurements as a function of temperature. In the first thermal cycle, at 25 ºC the conductivity (σ) measured for protein/AgI-NPs was $\sigma \sim 8.1 \times 10^{-5}$ S/cm. During the heating process the ionic conductivity increases progressively and at 170 ºC the ionic conductivity reached $\sigma \sim 0.19$ S/cm (Fig. 7A). In the second thermal cycle, the conductivity at 25 ºC and 170 ºC were $\sim 1.7 \times 10^{-4}$ S/cm and 0.14 S/cm,

respectively (Fig. 7B). The difference observed in conductivity at room temperature (25 ^{o}C) between the two thermal cycles can be related mainly to the elimination of residual water (during the first heating process) confined in the protein layer even after the drying process. The conductivity at room temperature for protein/AgI-NPs (second thermal cycle) was one and two orders of magnitude lower than the conductivity observed for AgI nanoplates ($\sigma \sim 2.2 \times 10^{-3}$ S/cm) and PVP-coated AgI-NPs ($\sigma \sim 1.5 \times 10^{-2}$ S/cm), respectively [9,27]. However, the conductivity for protein/AgI-NPs at room temperature was three orders of magnitude higher than that of bulk AgI ($\sigma \sim 1.6 \times 10^{-7}$ S/cm). At 170 ^{o}C, the conductivity of protein/AgI-NPs ($\sigma \sim 0.14$ S/cm) is similar to that of PVP-coated AgI-NPs ($\sigma \sim 0.3$ S/cm) [9]. During the cooling process, the ionic conductivity remained very high, consistent with the presence of superionic α-phase, and returning to the initial value (value observed before the heating process) at 25 ^{o}C. The ionic conductivity measurements for protein/AgI-NPs are reproducible in a second thermal cycle as shown in Fig. 7B. In addition, a second analyzed sample showed slightly lower conductivity (data not shown) due to the different amounts of protein covering the AgI-NPs (precipitation of unbound proteins resulting from insufficient washing) and/or vacancies as also observed for PVP-coated AgI-NPs [10].

The Ag^{+} ions mobility in the protein/AgI-NPs could be facilitated by the iodine anions locked on the AgI-NPs surface [9,14]. The amide group, in a peptide bond or ionizable functional groups in the sidechains of the amino acid residues can create well-defined conduction/diffusion paths for Ag^{+} ions due to a preferred binding tendency between organic portion and silver ions, which forms -$CONH_2$-Ag^{+} complex. Furthermore, the conduction of Ag^{+} ions by hopping effect is most likely promoted by the native structure of the protein. The conductivity data reported for protein/AgI-NPs were better when compared to the results reported by Fu and coworkers (using salt and

denatured proteins mixture) [14], which is attributed to the rigid structure of the native protein in association with the surface of the AgI-NPs. Up to now, the hypotheses on the complex phase transition of AgI coated by organic layer (be it polymer or protein) are based on factors such as scale decrease, facilitated interface interaction, and presence of defects. Uvarov and coworkers proved that the enhanced ionic conductivity in AgI/Al_2O_3 was a consequence of high concentrations of defects caused by silver vacancies in the interfacial region formed at the insulator/conductor interface, corroborating the ion transport model at the protein-coated AgI NPs [28]. Although the mechanism responsible for the pronounced conductivity is not well understood, it is reasonable to consider that the space charge regions between AgI and the insulating protein covering play an important role, since the conductivity of hybrid materials is governed mainly by the ionic transport via interface regions of the ionic crystal [21]. Thus, we assumed that the large interfacial area between the protein/AgI capping and the high amount of Ag^+ mobile ions may had led to the increase of the ionic conductivity in our system. Most of the defects enhance the ionic conductivity relating to monocrystalline phase, so the protein crystallization on as-synthesized AgI NPs surface can add more dislocations, vacancies, and thus increase the superionic conductivity.

The Fig. 8 shows a schematic illustration of the partial arrangement of the protein layer in contact with the AgI NPs, as previously suggested. The Fig. 8B suggests the possible mechanism of Ag^+ mobility between the semiconductor surface and the amino acids from protein insulator layer by ion hopping process. In a hopping mechanism, the peptide backbone connects the Ag^+ donor and acceptor and involves its amino acids in oxidation and reduction, creating regions in which the charge transfer is facilitated [29]. The maintenance of the superionic conductivity of the protein-coated

AgI NPs at lower temperatures has potential for technological applications in nanobatteries, highly selective chemical sensors, as a medium for optical information or image storage and other electrochemical devices [30-33]. Furthermore, the synthesized protein/AgI-NPs have the extended applications due to the presence of protein coating. We were able to maintain all the properties of the silver halide on the nanometric scale and added to them the advantages obtained by the protein corona. We can emphasize that the synthesized protein/AgI-NPs may promote drug targeting ability, act as directed target, and as drug delivery carriers, and how they are thermally stable have their applications potential expanded in different systems [30-33]. Interestingly, Wang and co-workers reported applications for cancer cell detection based on chitosan-modified silver halide nanoparticles with dual responsive enzyme mimetic activities [33]. Recalling that nanocomposites composed of iodine absorb strongly X-rays, various iodine compounds coated with inert or biocompatible material (such as silica and protein corona) have arisen to increase the contrast of X-ray images, as proposed in works of Kobayashi and co-workers and Yang and co-workers [35-37]. Similarly, we can hypothesize that the synthesis proposed in this study guarantees to protein/AgI-NPs similar biotechnological applications.

4. Conclusion

It is noteworthy that this study showed for the first time not only a high conductivity of the obtained protein-coated AgI nanoparticles, but also an ultrafast and facile photochemical route under mild conditions to obtain them. Also, the manipulation of protein-coated AgI nanoparticles can be facilitated by the presence of a protein layer,

since the different chemical groups can be used in the interface reactions that allow the use in various technological fields. The role of protein as template and stabilizer encourages the study of this class of biomolecules in the synthesis of new superionic nanoconductors. Furthermore, the type of synthesis proposed here may boost the growth of physicochemical studies such as ionic mobility and phase predominance in silver halide nanoparticles not reported so far. Our results showed excellent superionic conductivity for protein/AgI-NPs with the transition from the α- to β/γ- phase drastically suppressed towards lower temperature. The conductivity and phase transition were reproducible during the thermal cycles, indicating stability of the protein layer throughout the process. The maintenance of the superionic conductivity of the protein-coated AgI nanoparticles at lower temperatures has potential for technological applications in electrochemical devices. Furthermore, protein-coated AgI NPs have great potential for biotechnological and biomedical applications.

Conflict of Interest. The authors declare no conflict of interest.

Funding. This study was funded by Fundação de Amparo à Pesquisa do Estado de São Paulo (FAPESP) via grants number 2017/17275-3 and 2017/16976-8, and also by Conselho Nacional de Desenvolvimento Cientifico e Tecnológico (CNPq) via grant number 402289/2013-7, 307664/2015-5 and 305740/2017-2.

Acknowledgements. The authors are grateful to the Multiuser Central Facilities (UFABC) for the experimental support.

References

[1] B.B. Owens, Solid state electrolytes: Overview of materials and applications during the last third of the Twentieth Century, J. Power Sources. 90 (2000) 2–8. doi:10.1016/S0378-7753(00)00436-5.

[2] M. Armand, J.M. Tarascon, Building better batteries, Nature. 451 (2008) 652–657. doi:10.1038/451652a.

[3] P. Simon, Y.M. Gogotsi, Materials for electrochemical capacitors, Nat. Mater. 7 (2008) 845–854. doi:10.1038/nmat2297.

[4] Y. Kato, S. Hori, T. Saito, K. Suzuki, M. Hirayama, A. Mitsui, M. Yonemura, H. Iba, R. Kanno, High-power all-solid-state batteries using sulfide superionic conductors, Nat. Energy. 1 (2016) 16030. doi:10.1038/nenergy.2016.30.

[5] G. Burley, Structure of hexagonal silver iodide, J. Chem. Phys. 38 (1963) 2807–2812. doi:10.1063/1.1733606.

[6] T. Takahashi, K. Kuwabara, O. Yamamoto, The Electrical Conductivity and the Crystal Structure of Silver Iodide, J. Electrochem. Soc. - J Electrochem SOC. 116 (1969).

[7] B.J. Morgan, P.A. Madden, Relationships between atomic diffusion mechanisms and ensemble transport coefficients in crystalline polymorphs, Phys. Rev. Lett. 112 (2014). doi:10.1103/PhysRevLett.112.145901.

[8] S. Hull, Superionics: Crystal structures and conduction processes, Reports Prog. Phys. 67 (2004) 1233–1314. doi:10.1088/0034-4885/67/7/R05.

[9] R. Makiura, T. Yonemura, T. Yamada, M. Yamauchi, R. Ikeda, H. Kitagawa, K. Kato, M. Takata, Size-controlled stabilization of the superionic phase to room temperature in polymer-coated AgI nanoparticles, Nat. Mater. 8 (2009) 476–480. doi:10.1038/nmat2449.

[10] T. Yamamoto, M. Maesato, N. Hirao, S.I. Kawaguchi, S. Kawaguchi, Y. Ohishi, Y. Kubota, H. Kobayashi, H. Kitagawa, The room-temperature superionic conductivity of silver iodide nanoparticles under pressure, J. Am. Chem. Soc. 139 (2017) 1392–1395. doi:10.1021/jacs.6b11379.

[11] T. Yamamoto, H. Kobayashi, L.S.R. Kumara, O. Sakata, K. Nitta, T. Uruga, H. Kitagawa, Disappearance of the Superionic Phase Transition in Sub-5 nm Silver Iodide Nanoparticles, Nano Lett. 17 (2017) 5273–5276. doi:10.1021/acs.nanolett.7b01535.

[12] R.R. Naik, S.J. Stringer, G. Agarwal, S.E. Jones, M.O. Stone, Biomimetic synthesis and patterning of silver nanoparticles, Nat. Mater. 1 (2002) 169–172. doi:10.1038/nmat758.

[13] J.N. Araújo, A. Tofanello, V.M. da Silva, J.A.P. Sato, F.M. Squina, I.L. Nantes,

W. Garcia, Photobiosynthesis of stable and functional silver/silver chloride nanoparticles with hydrolytic activity using hyperthermophilic β-glucosidases with industrial potential, Int. J. Biol. Macromol. 102 (2017) 84–91. doi:https://doi.org/10.1016/j.ijbiomac.2017.04.001.

[14] X. Fu, Y. Jewel, Y. Wang, J. Liu, W.H. Zhong, Decoupled Ion Transport in a Protein-Based Solid Ion Conductor, J. Phys. Chem. Lett. 7 (2016) 4304–4310. doi:10.1021/acs.jpclett.6b02071.

[15] R. Hong, T. Pan, J. Qian, H. Li, Synthesis and surface modification of ZnO nanoparticles, Chem. Eng. J. 119 (2006) 71–81. doi:10.1016/j.cej.2006.03.003.

[16] M.G. Jeong, H.O. Seo, K.D. Kim, D.H. Kim, Y.D. Kim, D.C. Lim, Quenching of photocatalytic activity and enhancement of photostability of ZnO particles by polydimethysiloxane coating, J. Mater. Sci. 47 (2012) 5190–5196. doi:10.1007/s10853-012-6402-6.

[17] N. Jain, A. Bhargava, J. Panwar, Enhanced photocatalytic degradation of methylene blue using biologically synthesized “protein-capped” ZnO nanoparticles, Chem. Eng. J. 243 (2014) 549–555. doi:10.1016/j.cej.2013.11.085.

[18] D.F. Vieira, C.O. Avellaneda, A. Pawlicka, Conductivity study of a gelatin-based polymer electrolyte, Electrochim. Acta. 53 (2007) 1404–1408. doi:10.1016/j.electacta.2007.04.034.

[19] T. Basu, M.M. Goswami, T.R. Middya, S. Tarafdar, Morphology and ion-conductivity of gelatin-LiClO4 films: Factional diffusion analysis, J. Phys. Chem. B. 116 (2012) 11362–11369. doi:10.1021/jp306205h.

[20] A. Ghadami, N. Taheri Qazvini, N. Nikfarjam, Ionic conductivity in gelatin-based hybrid solid electrolytes: The non-trivial role of nanoclay, J. Mater. Sci. Technol. 30 (2014) 1096–1102. doi:10.1016/j.jmst.2014.06.008.

[21] L.F. Liu, S.W. Lee, J.B. Li, M. Alexe, G.H. Rao, W.Y. Zhou, J.J. Lee, W. Lee, U. Gösele, Enhanced ionic conductivity of AgI nanowires/AAO composites fabricated by a simple approach, Nanotechnology. 19 (2008). doi:10.1088/0957-4484/19/49/495706.

[22] F. Colussi, V.M. Da Silva, I. Miller, J. Cota, L.C. De Oliveira, M. De Oliveira Neto, F.M. Squina, W. Garcia, Oligomeric state and structural stability of two hyperthermophilic β-glucosidases from Thermotoga petrophila, Amino Acids. 47 (2015) 937–948. doi:10.1007/s00726-015-1923-3.

[23] J. Cota, T.L.R. Corrêa, A.R.L. Damásio, J.A. Diogo, Z.B. Hoffmam, W. Garcia, L.C. Oliveira, R.A. Prade, F.M. Squina, Comparative analysis of three hyperthermophilic GH1 and GH3 family members with industrial potential, N. Biotechnol. 32 (2015) 13–20. doi:10.1016/j.nbt.2014.07.009.

[24] H. Yu, L. Liu, X. Wang, P. Wang, J. Yu, Y. Wang, The dependence of photocatalytic activity and photoinduced self-stability of photosensitive AgI nanoparticles, Dalt. Trans. 41 (2012) 10405–10411. doi:10.1039/c2dt30864a.

[25] P.S. Kumar, P.B. Dayal, C.S. Sunandana, On the formation mechanism of γ-AgI

thin films, Thin Solid Films 357 (1999) 111–118. doi: 10.1016/S0040-6090(99)00647-1.

[26] S. Yamasaki, T. Yamada, H. Kobayashi, H. Kitagawa, Preparation of sub-10 nm AgI nanoparticles and a study on their phase transition temperature, Chem. - An Asian J. 8 (2013) 73–75. doi:10.1002/asia.201200790.

[27] Y.G. Guo, J.S. Lee, J. Maier, Agi nanoplates with mesoscopic superionic conductivity at room temperature, Adv. Mater. 17 (2005) 2815–2819. doi:10.1002/adma.200501215.

[28] N.F. Uvarov, P. Vanek, M. Savinov, V. Zelezny, V. Studnicka, J. Petzelt., Percolation effect, thermodynamic properties of AgI and interface phases in AgI-Al_2O_3 composites, Solid State Ion. 127 (2000) 253–267. doi: 10.1016/S0167-2738(99)00288-X.

[29] A.A. Voityuk, B.J. Lee, Long-range electron transfer in biomolecules. Tunneling or hopping?, J. Phys. Chem. B. 115 (2011) 12202–12207. doi: 10.1021/jp2054876.

[30] V.H. Nguyen, B.J. Lee, Protein corona: A new approach for nanomedicine design, Int. J. Nanomedicine. 12 (2017) 3137–3151. doi:10.2147/IJN.S129300.

[31] Z. Jingbin, L. Min, L. Ao, F. Fan, Z. Teng, D. Wei, L. Mengmeng, G. Mingfu, W. Cong-Ying, Y. Yadong, Au/AgI Dimeric Nanoparticles for Highly Selective and Sensitive Colorimetric Detection of Hydrogen Sulfide, Adv. Funct. Mater. 28 (n.d.) 1800515. doi:10.1002/adfm.201800515.

[32] M. Rioux, Y. Ledemi, Y. Messaddeq, An experimental study of the effect of AgI on the optical and electrical properties of conductive glasses in the system AgI-AgPO3-WO3, J. Non. Cryst. Solids. 459 (2017) 169–175. doi:https://doi.org/10.1016/j.jnoncrysol.2017.01.011.

[33] G.L. Wang, X.F. Xu, L. Qiu, Y.M. Dong, Z.J. Li, C. Zhang, Dual responsive enzyme mimicking activity of AgX (X = Cl, Br, I) nanoparticles and its application for cancer cell detection, in: ACS Appl. Mater. Interfaces, 2014: pp. 6434–6442. doi:10.1021/am501830v.

[34] Y. Kobayashi, T. Ayame, T. Nakagawa, Y. Kubota, K. Gonda, N. Ohuchi, Preparation of AgI/Silica/Poly(Ethylene Glycol) Nanoparticle Colloid Solution and X-Ray Imaging Using It, ISRN Nanomater. 2013 (2013) 1–5. doi:10.1155/2013/670402.

[35] Y. Kobayashi, M. Minato, K. Ihara, M. Sato, N. Suzuki, M. Takeda, N. Ohuchi, A. Kasuya, Synthesis of silica-coated AgI nanoparticles and immobilization of proteins on them, J Nanosci Nanotechnol. 10 (2010) 7758–7761. doi:10.1166/jnn.2010.2838.

[36] O. Anamaria, Y. Yi, F. Ting, W. Xueding, W. Hui, L. Yuancheng, Y. Lily, T. Xiangyang, M. Hui, A nanocomposite of Au-AgI core/shell dimer as a dual-modality contrast agent for x-ray computed tomography and photoacoustic imaging, Med. Phys. 43 (n.d.) 589–599. doi:10.1118/1.4939062.

[37] Y. Kobayashi, K. Misawa, M. Takeda, M. Kobayashi, M. Satake, Y. Kawazoe,

N. Ohuchi, A. Kasuya, M. Konno, Silica-coating of AgI semiconductor nanoparticles, Colloids Surfaces A Physicochem. Eng. Asp. 251 (2004) 197–201. doi:10.1016/j.colsurfa.2004.10.007.

Figures legends

Fig. 1. Photosynthesis of protein/AgI-NPs. (**A**) Electronic absorption spectra of protein/AgI-NPs as a function of time under blue light irradiation. Left inset: electromagnetic spectra emitted by the blue light source. Right inset: absorbance at 420 nm as a function of time. The solid line is just a guide for the eye. (**B**) Vial 1 (control): ultrapure water under blue light irradiation. Vial 2 (control): ultrapure water containing 1 mM $AgNO_3$ under blue light irradiation. Vial 3 (control): ultrapure water containing 1 mM KI under blue light irradiation. Vial 4 (control): ultrapure water containing 1 mM $AgNO_3$ + 1 mM KI under blue light irradiation. Vial 5: ultrapure water containing 1 mM $AgNO_3$ + 1 mM KI + 2 μM β-glucosidase GH1 under blue light irradiation.

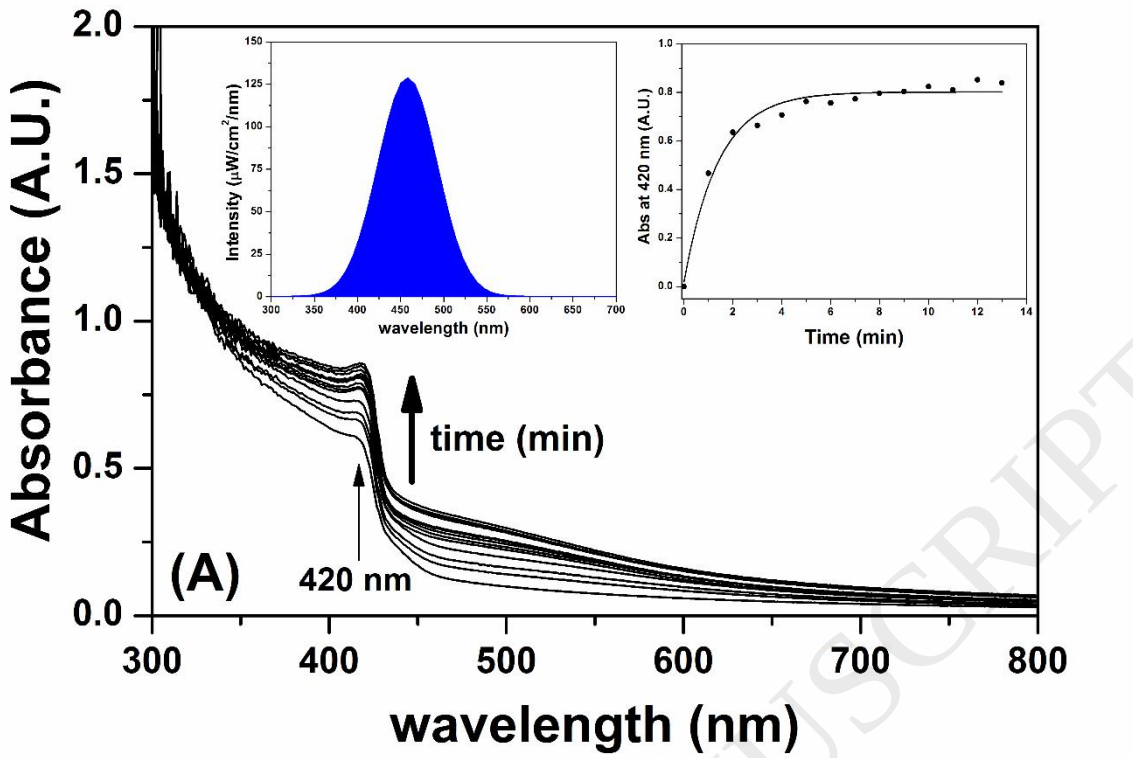

(B)

Fig. 2. Transmission electron microscopy (TEM) of protein/AgI-NPs. Left: a representative transmission electron micrograph showing protein/AgI-NPs. Right: particle size distribution histogram of protein/AgI-NPs, mean diameter of 12.8 ± 4.9 nm. The total number of nanoparticles counted was 1,500.

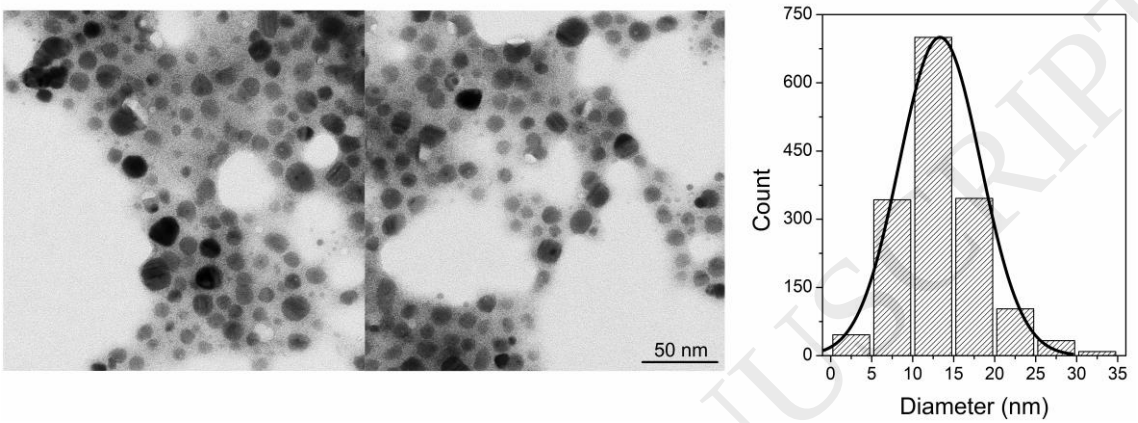

Fig. 3. Size distribution histogram of the distances between the AgI NPs. The mean distance was 7.5 ± 1.5 nm. The total number of distances counted was 210.

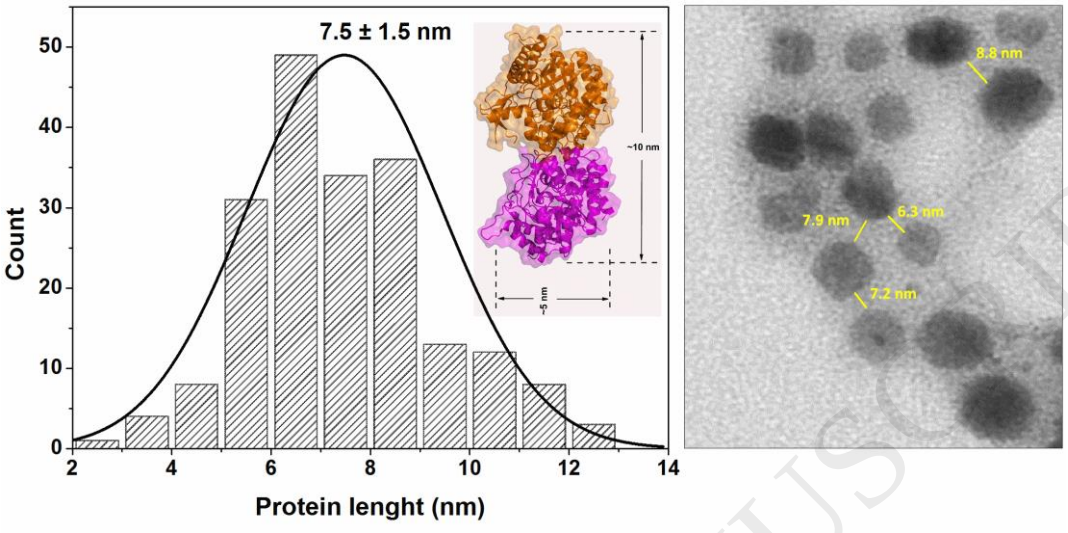

Fig. 4. Differential scanning calorimetry (DSC) thermograms of protein/AgI-NPs for four consecutive thermal cycles (heating/cooling processes). The data for the protein/AgI-NPs sintered at 450 ºC for 4 hours are also included at the bottom for comparison.

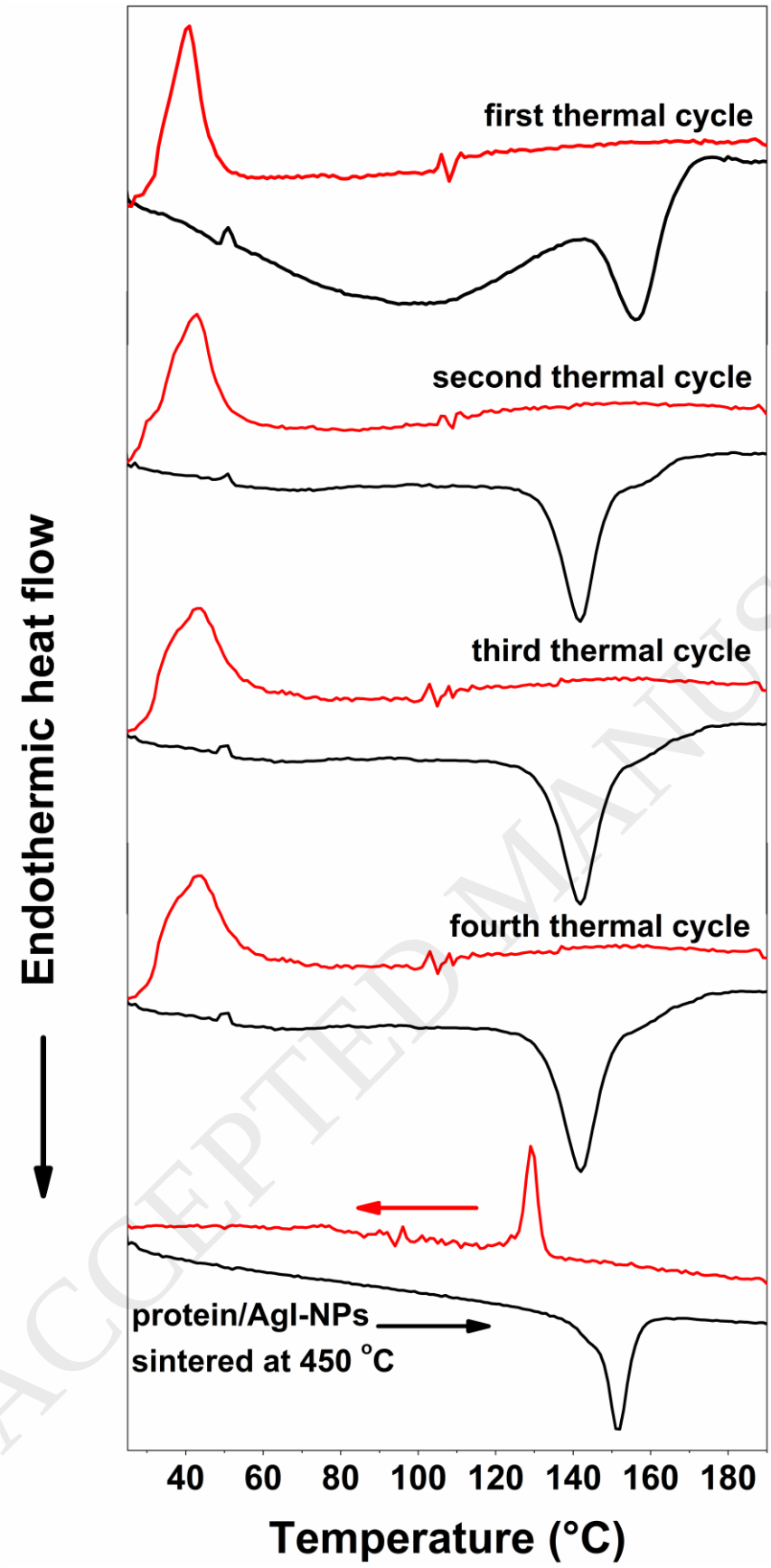

Fig. 5. X-ray powder diffraction (XRD) patterns for protein/AgI-NPs during thermal cycling.

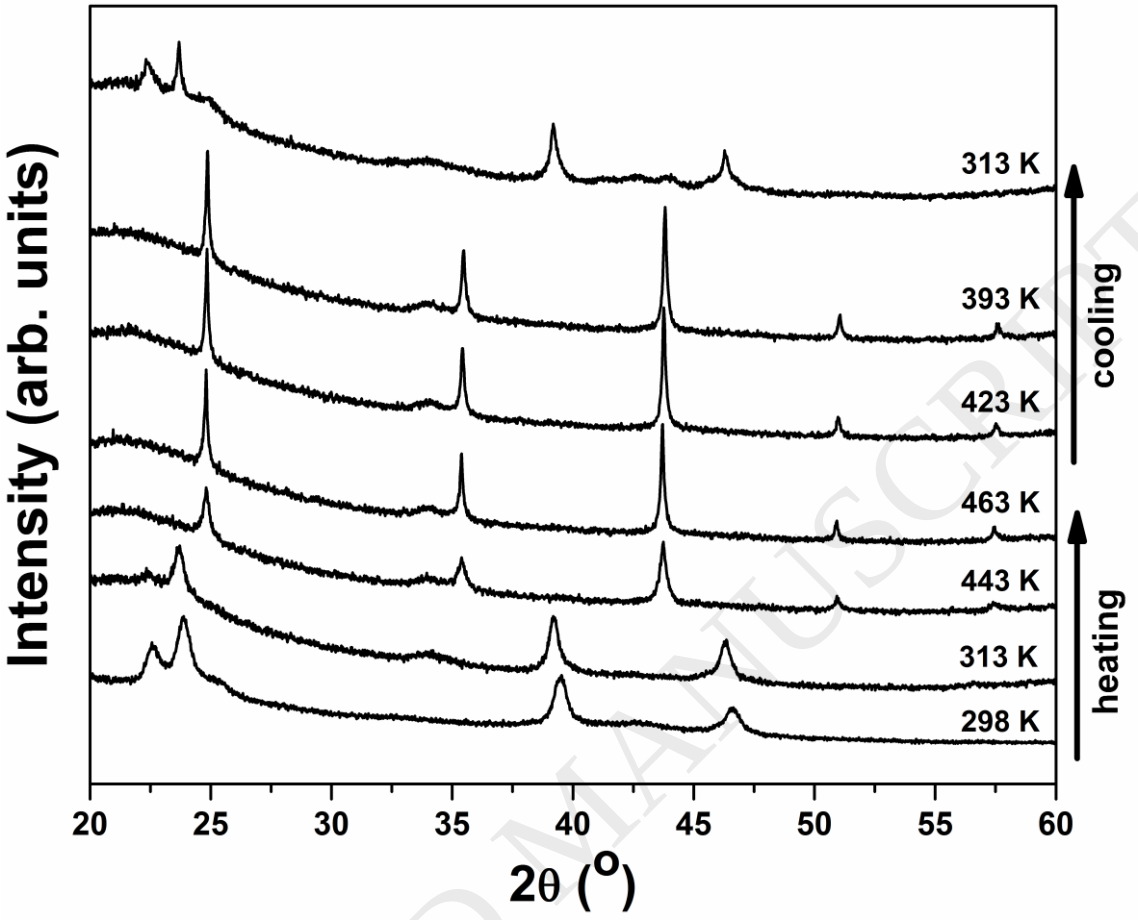

Fig. 6. Rietveld plot of the protein/AgI-NPs sample measured at 25 ºC. The observed pattern is represented by the black open circles while the calculated pattern is indicated by the red line. The difference between the calculated and observed pattern is displayed by the blue line at the bottom. The vertical bars indicate the Bragg peaks of both β-AgI and γ-AgI phases.

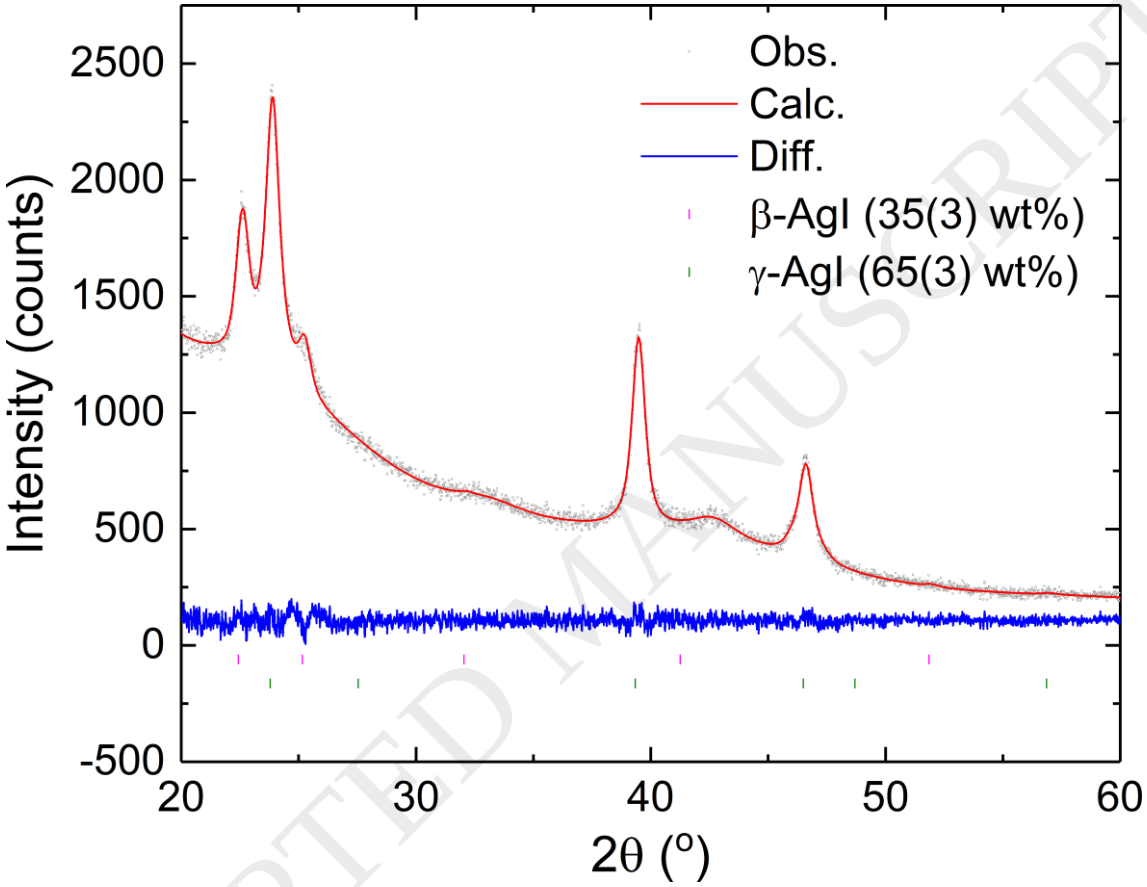

Fig. 7. Transport behavior of protein/AgI-NPs. Temperature dependence of the conductivity (σ) for two consecutive thermal cycles.

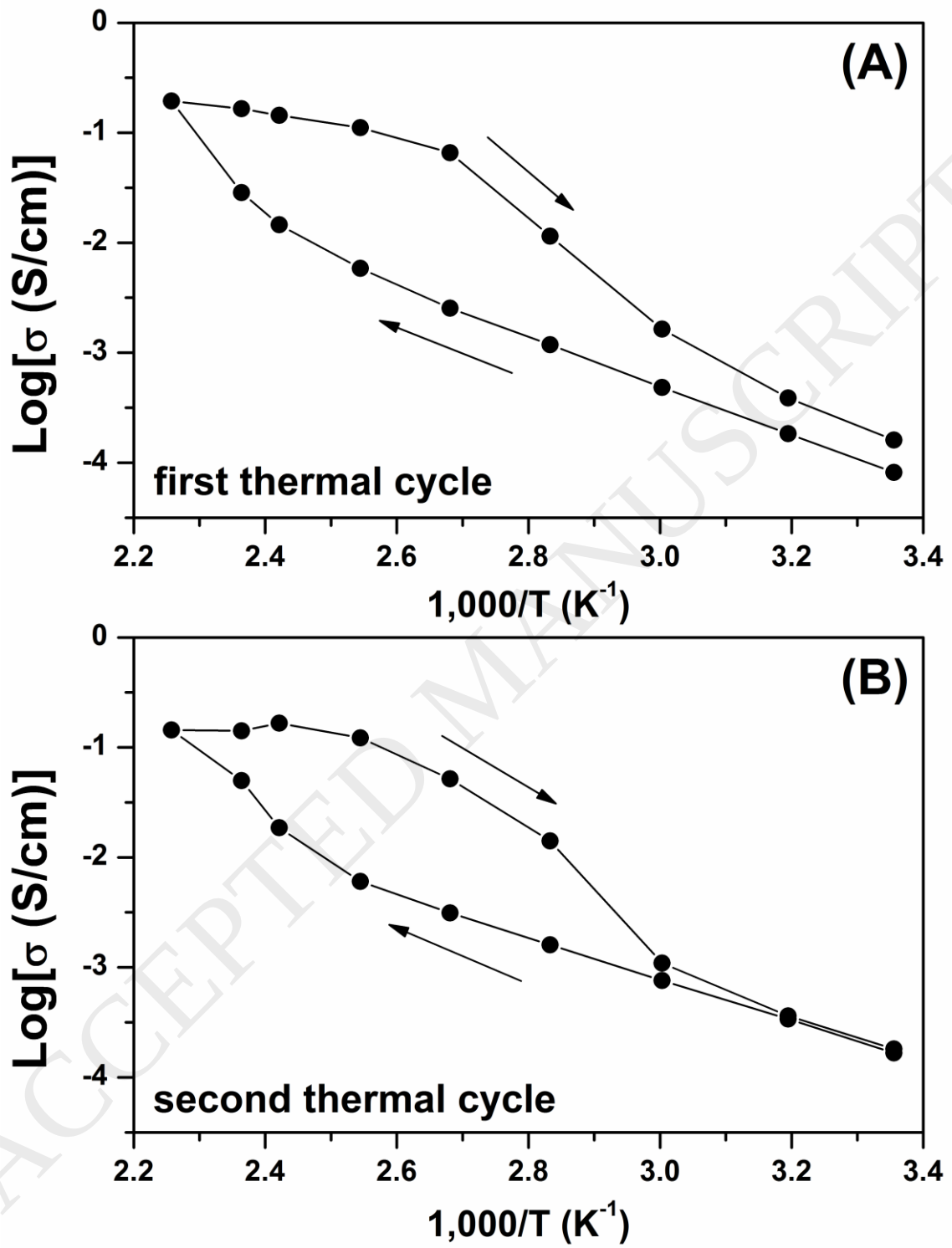

Fig. 8. Schematic illustration of the arrangement of the protein layer on the AgI nanoparticle surface. (**A**) Illustration of protein bilayer. (**B**) Amino acids create well-defined conduction/diffusion paths for Ag^+ ions.